Magnetoresistance in an All-Organic-Based Spin Valve

*Bin Li, Chi-Yueh Kao, Jung-Woo Yoo, Vladimir N. Prigodin, and Arthur J. Epstein**

Spintronics is the new paradigm of electronics and utilizes the spin degree of freedom of the electron.[1] In addition to metal-based spintronic devices, which already have wide applications (e.g., read heads of hard disk drives), semiconductor spintronics provides the possibility to combine logic, communication, and storage operation using hybrid devices.[2] Recently, spintronic devices based on organic materials have attracted much attention because of the potential long spin lifetime due to low spin-orbit coupling and weak hyperfine interaction, as well as the ability to fabricate low-cost, light-weight, and mechanically flexible devices.[3–9] Organic semiconductors have been used as the spacers in spin valve devices with ferromagnetic metal or transitional metal oxide contacts. One fundamental obstacle for spin injection from a ferromagnetic metal into a semiconductor is the conductivity mismatch.[10] The development of fully spin-polarized magnetic semiconductors offers a promising route to circumvent this problem. Organic-based magnets such as $V[TCNE]_x$ ($x \approx 2$, TCNE: tetracyanoethylene) provide advantages including high magnetic ordering temperature, fully spin-polarized semiconducting electronic structure, chemical tunability, and low-temperature processing.[11] Here, we show results for spin injection and detection in an all-organic-based spin valve using the organic magnetic semiconductor $V[TCNE]_x$ as both the spin injector and analyzer. We observed unusual inverted spin valve effect and propose that the negative magnetoresistance (MR) originates from the spin-dependent tunneling between highly spin-polarized bands split by Coulomb interaction.

$V[TCNE]_x$ is the first reported room-temperature molecule-based magnet with magnetic ordering temperature $T_C \approx 400$ K.[12] The magnetic order originates from the antiferromagnetic coupling between the three unpaired electrons of the V^{2+} ion in $3d(t_{2g})$ orbitals with a total spin $S = 3/2$ and the unpaired electrons of the $[TCNE]^-$ anion in π^* orbital with $s = 1/2$.[13] Stoichiometry shows that there is approximately one V^{2+} ion on average for two $[TCNE]^-$ anions, leading to a net spin of 1/2 for the repeat unit (**Figure 1**). This high-T_C magnetic material

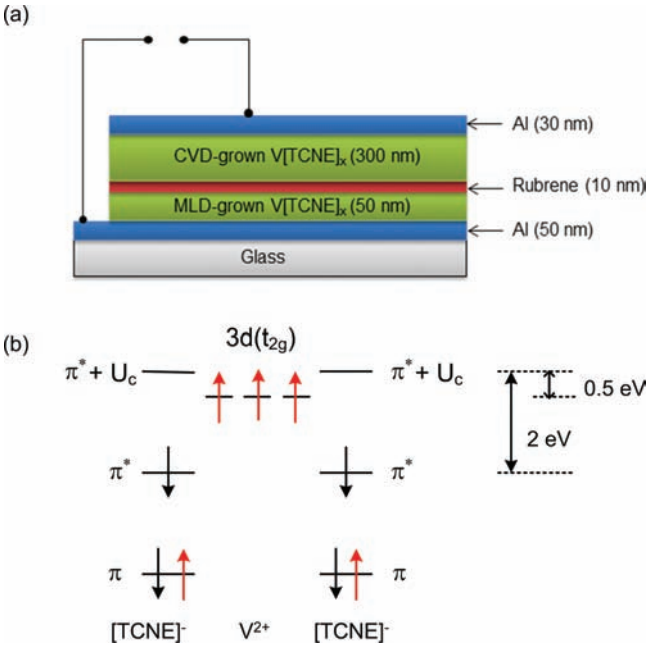

Figure 1. a) Device structure and b) schematic view of the energy levels of $V[TCNE]_x$ ($x \approx 2$).

can be prepared as powder in dichloromethane[12] or grown as a thin film by low-temperature (≈40 °C) chemical vapor deposition (CVD).[14] Extended X-ray absorption fine structure (EXAFS) analysis showed that each vanadium ion is coordinated by six nitrogen atoms at a room-temperature average distance of 2.084(5) Å, suggesting strong binding between V and TCNE.[15] Recently, a molecular layer deposition (MLD) method has been developed for $V[TCNE]_x$ films.[16] MLD is able to precisely control the thickness of the film within a monolayer by exposing the substrate alternatively and sequentially to different precursors.[16] $V[TCNE]_x$ has a unique half-semiconductor electronic structure with fully spin-polarized valence and conduction bands.[11,13] Because of the on-site Coulomb repulsion U_c, the π^* level of $[TCNE]^-$ is split into two sublevels, occupied π^* and unoccupied $\pi^* + U_c$, with opposite spin polarizations. It was shown that the energy split between the π^* and the $\pi^* + U_c$ levels is approximately 2 eV.[17] Results of photoelectron spectroscopy (PES) and resonant photoemission (RPE) studies suggested that the occupied π^* level lies about 1.5 eV below the V(3d) state, while the unoccupied $\pi^* + U_c$ level is 0.5 eV higher than the V(3d) state.[18] An activation energy of 0.5 eV is determined from the temperature dependence of the conductivity for a CVD-prepared thin film, coinciding with the energy

B. Li, Dr. J.-W. Yoo, Prof. V. N. Prigodin, Prof. A. J. Epstein
Department of Physics
The Ohio State University
Columbus, OH 43210–1117, USA
E-mail: epstein@physics.osu.edu
C.-Y. Kao, Prof. A. J. Epstein
Department of Chemistry
The Ohio State University
Columbus, OH 43210–1173, USA
Prof. V. N. Prigodin
Ioffe Institute
194021 St. Petersburg, Russia

DOI: 10.1002/adma.201100903

difference between the 3d(t_{2g}) and $\pi^* + U_c$ levels.[13] The activation energy of MLD films is approximately 0.4 eV, slightly lower than that of CVD film.[16]

As shown in Figure 1, the overall structure of the device is, starting from the bottom: Al/V[TCNE]$_x$/rubrene/V[TCNE]$_x$/Al. The V[TCNE]$_x$ films serve as two ferromagnetic (FM) contacts with different coercive fields while the organic semiconductor rubrene ($C_{42}H_{28}$) is used as the spacer. Al (50 nm) is deposited on clean glass substrates as the electrodes. The V[TCNE]$_x$ film grown by MLD (40 layers, ≈50 nm) serves as the bottom FM layer. Rubrene is well known for its high charge mobility and has been demonstrated to be an efficient tunnel barrier.[7,8] 10 nm of rubrene is thermally evaporated on top of MLD-grown V[TCNE]$_x$ using an effusion cell. The thickness of the rubrene layer is within the tunneling regime (<15 nm) previously reported.[19] Another V[TCNE]$_x$ (300 nm) film grown by CVD is used as the top FM layer. Al (30 nm) is then deposited as the top electrode. The injected carriers are polarized by the first V[TCNE]$_x$ layer encountered and then tunnel through the barrier, reaching the second V[TCNE]$_x$ which acts as the analyzer. The magnetization hysteresis curves of the two V[TCNE]$_x$ films are recorded separately using a superconducting quantum interference device (SQUID). In a spin valve, the device resistance depends on the relative magnetization direction (parallel or antiparallel) of the two FM layers. The MR is defined as $MR = (R_{AP} - R_P)/R_P$, where R_{AP} and R_P are the device resistances corresponding to antiparallel and parallel configuration, respectively.

The measurements were performed between 10 K and 300 K. **Figure 2** shows the current–voltage (I–V) characteristics for the spin valve device with the structure of Al(50 nm)/V[TCNE]$_x$(50 nm)/rubrene(10 nm)/V[TCNE]$_x$(300 nm)/Al (30 nm). The I–V curves are nonlinear and strongly temperature dependent, similar to the reported LSMO/rubrene/V[TCNE]$_x$ tunnel junction.[11] Figure 2 also presents the temperature dependence of the normalized device resistance with comparison to the bulk resistances of the CVD-grown and MLD-grown

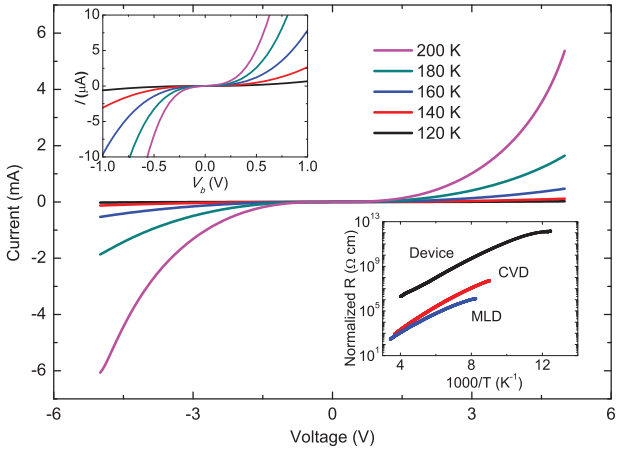

Figure 2. I–V curves of the spin valve device at different temperatures. The upper inset shows enlarged figure near bias voltage V_b = 0 V. The lower inset shows the temperature-dependent resistances for the spin valve device (black) as well as the bulk resistance of V[TCNE]$_x$ films. The two V[TCNE]$_x$ films are deposited by CVD (red) and MLD (blue) respectively.

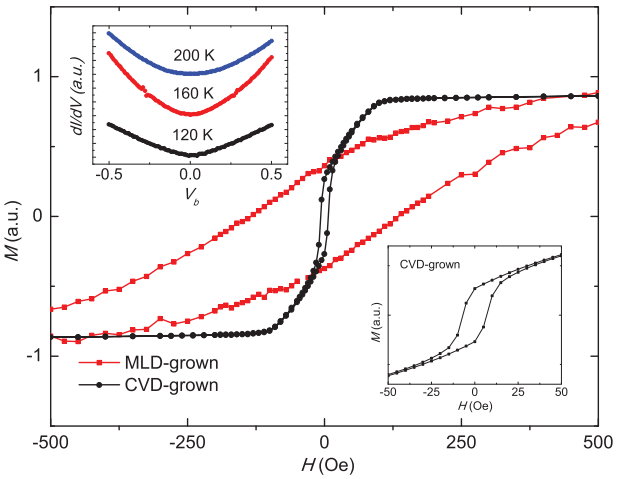

Figure 3. Magnetization hysteresis curves of V[TCNE]$_x$ films recorded by SQUID at a temperature T = 100 K. Red data sets denote the MLD-grown film and black curves represent the CVD-grown film. The lower inset shows enlarged hysteresis loop of CVD-grown film on a different scale. The upper inset shows the dI/dV curves for the tunnel junction at different temperatures.

V[TCNE]$_x$ films. At high temperatures, the current of the device is controlled by the injection of charge carriers between the organic magnets and the organic semiconductor. Below 100 K, the bulk resistances of V[TCNE]$_x$ films, which increase exponentially with decreasing temperature, start to dominate the total device resistance. The crossover between injection-limited regime and V[TCNE]$_x$ bulk-limited regime was also reported in a V[TCNE]$_x$-based hybrid device.[11] As shown in **Figure 3**, the dI/dV curves have similar shapes at different temperatures. As discussed in previous literature, the absence of the zero bias anomaly indicates that rubrene forms a good tunneling barrier.[4]

The magnetization hysteresis curves of the CVD-grown and MLD-grown V[TCNE]$_x$ films are presented in Figure 3. Note that the coercive field of the MLD-grown film is much larger than that of the CVD-grown sample. The MLD film was prepared at much slower deposition rate (≈0.98 nm per cycle) and the MLD film has larger density, which suggest that this increased coercive field is possibly due to more complete metal–ligand coordination as well as stronger coupling between V^{2+} and $[TCNE]^-$.[16] The variation of the device resistance as a function of the applied in-plane magnetic field recorded at 120 K and 4 V is shown in **Figure 4**. Clean and reproducible negative MR curves are obtained, which correspond well to the coercive fields of the FM layers. The higher coercive field is ascribed to MLD-grown V[TCNE]$_x$ and the lower field to the CVD-grown V[TCNE]$_x$. The device resistance depends on the relative alignment of the magnetization of the magnetic layers, as the parallel configuration resistance R_P differs from the antiparallel resistance R_{AP}. At high magnetic field larger than 100 Oe, the magnetic moments of the two FM layers align in parallel. As the external field is swept, the CVD-grown V[TCNE]$_x$ film switches its magnetic moment first, resulting an antiparallel configuration with a change of the device resistance. After the switch of the other FM layer, the device returns to parallel alignment.

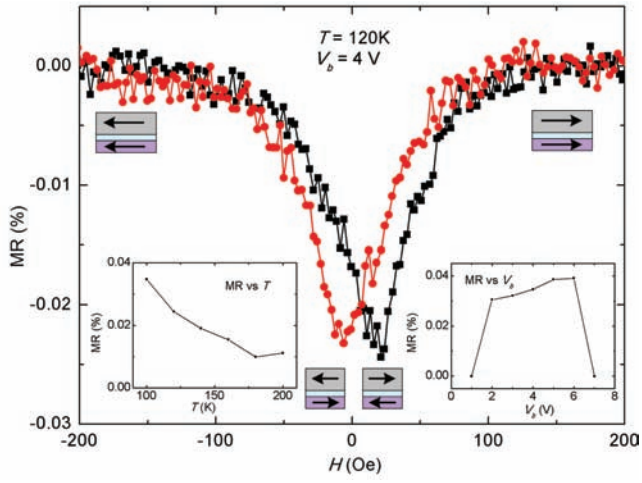

Figure 4. Magnetoresistance curve measured at 120 K with $V_b = 4$ V. The left inset shows the temperature dependence of the MR value with $V_b = 4$ V. The right inset shows the bias voltage dependence of the MR value at $T = 100$ K.

The maximum MR value of 0.04% is obtained at 100 K. Below 100 K, the device resistance is dominated by the bulk resistance of the $V[TCNE]_x$ films and becomes too large, thus it is difficult to detect any field-dependent interface resistance changes. The MR value deceases as temperature goes up, which was common in reported magnetic tunnel junctions and explained by the temperature dependence of the defect density.[7] The MR value varies slightly with bias, vanishing above 6 V. This negative MR is found to be independent of the bias polarity.

We observed the spin valve effect in 14 devices out of the total 16 devices fabricated, all of which showed inverted spin valve effect, with the low-resistance state corresponding to the antiparallel configuration. We note that both positive and negative MR effects have been reported in organic spin valves.[3,4,7,8,20–27] The inverted spin valve effect has been suggested to be due to ballistic channels from pinholes, which occur during the metal deposition on top of the organic semiconductor.[28,29] However, the fabrication process of our devices rules out this possibility because the rubrene is covered by a $V[TCNE]_x$ film prepared by CVD at low temperature (≈40 °C) rather than a thermally deposited ferromagnetic metal. The charge transport through $V[TCNE]_x$ will also preclude the metal migration and the formation of ballistic channels due to pinholes. Barraud et al. pointed out that for organic spin valves, the first molecule layer at the electrode interface plays a crucial role, and could even change the sign of the spin polarization of the FM electrode.[26] They proposed a spin-hybridization-induced polarized state (SHIPS) model with an "effective" spin polarization (P^*) due to the specific bonding of different band states of the FM electrodes at the organic interface.

The possibility that the rubrene layer contributes to the MR is also ruled out, because the organic magnetoresistance (OMAR)[30–36] originates from the bulk transport in organic semiconductors and our devices are dominated by tunneling through the 10 nm rubrene thin layer. In addition, the reported magnetoresistance of $V[TCNE]_x$ films are one order of magnitude smaller than the MR value obtained in our spin valve devices.[13,37] The negative sign of MR observed in our devices is independent of temperature and bias voltage, which is different from the previously reported MR results that a negative sign could be changed to positive with variation of the temperature and bias voltages.[22] We suggest that the negative MR in our devices is an intrinsic feature of $V[TCNE]_x$-related spin-polarized energy levels, as shown in **Figure 5**. Here we propose a simple phenomenological bias-enhanced selective tunneling (BEST) model to explain the negative MR. As an external bias

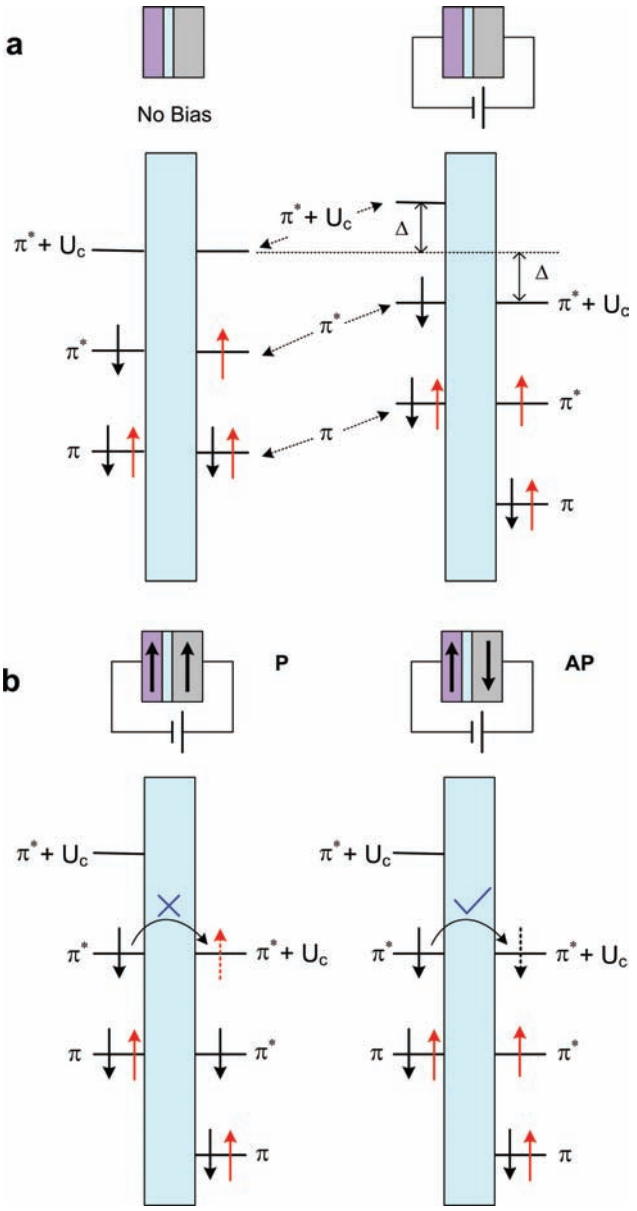

Figure 5. Simplified energy diagram for a $V[TCNE]_x$/rubrene/$V[TCNE]_x$ tunnel junction. a) The left shows the energy levels without external bias and the right presents the bias-induced level shifts (Δ is the energy shift due to applied bias). b) In the parallel configuration, the electron on the left π^* level cannot tunnel into the right $\pi^* + U_c$ level. This tunneling process can take place in the antiparallel alignment.

is applied to the device, the energy levels of the $V[TCNE]_x$/rubrene/$V[TCNE]_x$ junction are shifted. The effect of an external bias on the alignment of energy levels is shown schematically in Figure 5a, indicating that the energy of one $V[TCNE]_X$ film is raised up and the other is lowered due to applied external bias. At certain voltage, the π^* level of one $V[TCNE]_x$ contact is leveled with the energy of $\pi^* + U_c$ of the other $V[TCNE]_x$ contact. Note that the $3d(t_{2g})$ orbital is highly localized on the V^{2+} ion, while the π^* and $\pi^* + U_c$ orbitals are delocalized over the relatively large $[TCNE]^-$ anion due to π-conjugation.[38] We suggest that most of the tunneling happens between the π^* and the initially unoccupied $\pi^* + U_c$ levels. According to the Pauli exclusion principle, the allowable spin directions of the π^* and $\pi^* + U_c$ levels are opposite to each other (i.e., spin $\uparrow(\downarrow)$ in the π^* level while spin $\downarrow(\uparrow)$ in the $\pi^* + U_c$ level). When the magnetization of the two $V[TCNE]_x$ layers align parallel, the spins of the electrons on both of the π^* levels on each side are in same direction. As in Figure 5, the spin $\downarrow$ electron from the left π^* level tunnels through the barrier into the $\pi^* + U_c$ level on the other side. However, the allowable spin state on that $\pi^* + U_c$ level is spin $\uparrow$. As a result, this spin $\downarrow$ electron cannot enter that $\pi^* + U_c$ level and the device shows a high resistance. Under the antiparallel configuration, the spin $\downarrow$ electron from the left π^* level can tunnel into the $\pi^* + U_c$ level on the right, since the allowable state on that level is spin $\downarrow$. Thus, the device shows a low resistance. The bias dependence in the *I–V* curves related with the alignment of contact energy levels (Figure 2) is obscured by the field-dependent and phonon-assisted tunneling.[8] It is noted that the MR is independent of bias polarity, which is due to the same electronic structure of $V[TCNE]_x$ prepared by different deposition methods. We need to emphasize here that this energy level diagram is simplified. The details of the band structure still remain unclear. The energy level alignment of $V[TCNE]_x$ and other organic semiconductors still needs to be understood. It is noted that the possibility of the involvement of traps or impurity states is not ruled out. Additional careful studies should be conducted to uncover the details of the spin tunneling process.

In summary, we have reported clean and reproducible negative magnetoresistance in the device with a structure of $V[TCNE]_x$/rubrene/$V[TCNE]_x$. The results reflect successful spin injection and detection in an all-organic-based system and are explained by a new model of spin-dependent tunneling between the π^* and $\pi^* + U_c$ levels. The negative MR supports the significance of highly spin-polarized individual majority and minority bands with relatively narrow bandwidth due to strong on-site Coulomb interaction together with "weak" intermolecular overlap in molecular magnets. While the absolute MR values remain small, future investigation and optimization of the interfaces will offer more understanding of this system and opportunities to improve device performance. The results indicate the potential applications of organic magnetic semiconductors in flexible, light-weight, all-organic spintronic devices.

Acknowledgements

B.L. thanks Dr. Chia-Yi Chen for help with the CVD system. This work was supported in part by AFOSR Grant No. FA9550–06–1–0175, DOE Grant Nos DE-FG02–01ER45931, DE-FG02–86ER45271, NSF Grant No. DMR-0805220, the Center for Emergent Materials (an NSF-MRSEC; Award Number DMR-0820414) at The Ohio State University and the Institute for Materials Research at The Ohio State University.

Received: March 9, 2011
Revised: April 27, 2011
Published online:

[1] S. A. Wolf, D. D. Awschalom, R. A. Buhrman, J. M. Daughton, S. von Molnr, M. L. Roukes, A. Y. Chtchelkanova, D. M. Treger, *Science* **2001**, *294*, 1488.
[2] D. D. Awschalom, M. E. Flatte, *Nat. Phys.* **2007**, *3*, 153.
[3] Z. H. Xiong, D. Wu, Z. Valy Vardeny, J. Shi, *Nature* **2004**, *427*, 821.
[4] T. S. Santos, J. S. Lee, P. Migdal, I. C. Lekshmi, B. Satpati, J. S. Moodera, *Phys. Rev. Lett.* **2007**, *98*, 016601.
[5] S. Pramanik, C.-G. Stefanita, S. Patibandla, S. Bandyopadhyay, K. Garre, N. Harth, M. Cahay, *Nat. Nanotechnol.* **2007**, *2*, 216.
[6] W. J. M. Nabers, S. Faez, W. G. van der Wiel, *J. Phys. D: Appl. Phys.* **2007**, *40*, R205.
[7] J. H. Shim, K. V. Raman, Y. J. Park, T. S. Santos, G. X. Miao, B. Satpati, J. S. Moodera, *Phys. Rev. Lett.* **2008**, *100*, 226603.
[8] J.-W. Yoo, H. W. Jang, V. N. Prigodin, C. Kao, C. B. Eom, A. J. Epstein, *Phys. Rev. B.* **2009**, *80*, 205207.
[9] V. A. Dediu, L. E. Hueso, I. Bergenti, C. Taliani, *Nat. Mater.* **2009**, *8*, 707.
[10] G. Schmidt, D. Ferrand, L. W. Molenkamp, A. T. Filip, B. J. van Wees, *Phys. Rev. B.* **2000**, *62*, R4790.
[11] J.-W. Yoo, C.-Y. Chen, H. W. Jang, C. W. Bark, V. N. Prigodin, C. B. Eom, A. J. Epstein, *Nat. Mater.* **2010**, *9*, 638.
[12] J. M. Manriquez, G. T. Yee, R. S. McLean, A. J. Epstein, J. S. Miller, *Science*. **1991**, *252*, 1415.
[13] V. Prigodin, N. Raju, K. Pokhodnya, J. Miller, A. Epstein, *Adv. Mater.* **2002**, *14*, 1230.
[14] K. I. Pokhodnya, A. J. Epstein, J. S. Miller, *Adv. Mater.* **2000**, *12*, 410.
[15] D. Haskel, Z. Islam, J. Lang, C. Kmety, G. Srajer, K. I. Pokhodnya, A. J. Epstein, J. S. Miller, *Phys. Rev. B.* **2004**, *70*, 054422.
[16] C.-Y. Kao, J.-W. Yoo, A. J. Epstein, unpublished.
[17] C. Tengstedt, M. Unge, M. P. de Jong, S. Stafström, W. R. Salaneck, M. Fahlman, *Phys. Rev. B.* **2004**, *69*, 165208.
[18] C. Tengstedt, M. P. de Jong, A. Kanciurzewska, E. Carlegrim, M. Fahlman, *Phys. Rev. Lett.* **2006**, *96*, 057209.
[19] R. Lin, F. Wang, J. Rybicki, M. Wohlgenannt, K. A. Hutchinson, *Phys. Rev. B.* **2010**, *81*, 195214.
[20] F. J. Wang, C. G. Yang, Z. V. Vardeny, X. G. Li, *Phys. Rev. B.* **2007**, *75*, 245324.
[21] W. Xu, G. J. Szulczewski, P. LeClair, I. Navarrete, R. Schad, G. Miao, H. Guo, A. Gupta, *Appl. Phys. Lett.* **2007**, *90*, 072506.
[22] H. Vinzelberg, J. Schumann, D. Elefant, R. B. Gangineni, J. Thomas, B. Buchner, *J. Appl. Phys.* **2008**, *103*, 093720, .
[23] V. Dediu, L. E. Hueso, I. Bergenti, A. Riminucci, F. Borgatti, P. Graziosi, C. Newby, F. Casoli, M. P. De Jong, C. Taliani, Y. Zhan, *Phys. Rev. B* **2008**, *78*, 115203.
[24] Y. Liu, S. M. Watson, T. Lee, J. M. Gorham, H. E. Katz, J. A. Borchers, H. D. Fairbrother, D. H. Reich, *Phys. Rev. B.* **2009**, *79*, 075312.
[25] B. Li, J.-W. Yoo, C.-Y. Kao, H. W. Jang, C.-B. Eom, A. J. Epstein, *Org. Electron.* **2010**, *11*, 1149.
[26] C. Barraud, P. Seneor, R. Mattana, S. Fusil, K. Bouzehouane, C. Deranlot, P. Graziosi, L. Hueso, I. Bergenti, V. Dediu, F. Petroff, A. Fert, *Nat. Phys.* **2010**, *6*, 615.
[27] D. Sun, L. Yin, C. Sun, H. Guo, Z. Gai, X.-G. Zhang, T. Z. Ward, Z. Cheng, J. Shen, *Phys. Rev. Lett.* **2010**, *104*, 236602.
[28] T.-S. Kim, *Phys. Rev. B.* **2005**, *72*, 024401.
[29] S. Mukhopadhyay, I. Das, *Phys. Rev. Lett.* **2006**, *96*, 026601.

[30] T. L. Francis, O. Mermer, G. Veeraraghavan, M. Wohlgenannt, *New J. Phys.* **2004**, *6*, 185.
[31] O. Mermer, G. Veeraraghavan, T. L. Francis, Y. Sheng, D. T. Nguyen, M. Wohlgenannt, A. Köhler, M. K. Al-Suti, M. S. Khan, *Phys. Rev. B.* **2005**, *72*, 205202.
[32] V. Prigodin, J. Bergeson, D. Lincoln, A. Epstein, *Synth. Met.* **2006**, *156*, 757.
[33] P. A. Bobbert, T. D. Nguyen, F. W. A. vanOost, B. Koopmans, M. Wohlgenannt, *Phys. Rev. Lett.* **2007**, *99*, 216801.
[34] B. Hu, Y. Wu, *Nat. Mater.* **2007**, *6*, 985.
[35] J. D. Bergeson, V. N. Prigodin, D. M. Lincoln, A. J. Epstein, *Phys. Rev. Lett.* **2008**, *100*, 067201.
[36] B. Hu, L. Yan, M. Shao, *Adv. Mater.* **2009**, *21*, 1500.
[37] N. P. Raju, T. Savrin, V. N. Prigodin, K. I. Pokhodnya, J. S. Miller, A. J. Epstein, *J. Appl. Phys.* **2003**, *93*, 6799.
[38] A. Zheludev, A. Grand, E. Ressouche, J. Schweizer, B. G. Morin, A. J. Epstein, D. A. Dixon, J. S. Miller, *J. Am. Chem. Soc.* **1994**, *116*, 7243.